JOURNAL OF MATERIALS SCIENCE 22 (1987) 1457–1468

The prediction of R-curves and notched tensile strength for composite laminates

J. K. WELLS*, P. W. R. BEAUMONT
Cambridge University Engineering Department, Trumpington Street, Cambridge CB2 1PZ, UK

A new model is proposed to explain the cracking and fracture of notched composite laminates. It is based on the energy absorption associated with the micromechanisms of fracture. Crack-growth resistance curves (R-curves) are predicted for a wide range of laminate constructions and materials, and the corresponding notched strengths deduced. Both R-curve and notched strength predictions are in good agreement with published data. The effect of improved fibre–matrix bonding on laminate notched strength is investigated in a case-study, and is successfully predicted using the model.

1. Introduction

Several methods of predicting the tensile strength of notched composite laminates have been proposed. These include the "point" and "average" stress criteria [1, 2], the "inherent flaw" model [3] and numerous methods based on fracture mechanics. All the techniques predict a strength which varies, approximately, as the reciprocal of the square-root of the notch length, but all the equations contain at least one parameter which can be adjusted to fit the data.

This paper links the fundamental failure processes identified in single composite laminae [4, 5] to the propagation of macroscopic cracks in laminates. A simple model is derived which predicts crack growth resistance curves (R-curves) and notched tensile strength for composite laminates.

2. A simple model of laminate cracking

When a notched laminate is loaded in tension, a damage zone forms at the notch tip, extending as the load increases. At a critical load the crack propagates catastrophically. The crack path observed in the failed specimen is often complex; it may not be parallel to the original notch, and plies of different orientations may fracture in different directions. Fortunately, the symmetry and lay-up geometry of the laminate reduce the number of possible fracture paths.

The energy absorbed in this complex crack formation determines whether the crack propagates stably (and forms a crack-tip damage zone) or catastrophically. It is assumed that there is sufficient stress present to nucleate the cracks. This paper attempts to model these energy-absorbing processes.

Consider a laminate of $(+45/-45/0)_s$ construction as an example. A crack in each lamina is assumed to propagate in one of three directions, as shown in Fig. 1. These are directions in which a crack can readily propagate in at least one lamina, and will generally be parallel to fibres in the layers, or perpendicular to the applied load. For this material a value of $\theta = 45°$ is appropriate. For convenience the different directions are called Type 1, 2 or 3.

Consider now the plies in turn. In the outer ply ($+45°$) a Type 1 crack will split parallel to the fibres, which is a low-energy mode of propagation. A Type 2 crack would cut the fibres at 45° and a Type 3 at 90°. Both these directions would require more energy than Type 1 because they involve fibre fracture rather than matrix failure. The second ply ($-45°$) would split in a Type 3 direction, and fibres would break in Types 1 or 2.

In general, fracture of the $+45°$ ply would be dominated by Type 1 cracking and the $-45°$ ply by Type 3 cracking, since these are the lowest energy modes. However, to achieve this crack path the $+45°$ and $-45°$ plies must delaminate an area which lies between the two crack paths, as shown in Fig. 2. The delamination absorbs surface energy which will increase when the damage zone grows larger. As the crack advances, the amount of surface energy absorbed by delamination may be so large that it is energetically more favourable to fracture both plies by Type 2 cracking and therefore avoid the need for delamination.

The 0° plies at the centre of the laminate can fracture in any of the three crack directions with only small differences in energy (see Section 2.1). The symmetry of the laminate construction ensures that there is never a need to delaminate the centre plane of the laminate.

To determine the fracture path and to predict the energy absorbed by the cracking process requires the calculation of the energy absorbed in each of the 3^n possible fracture paths (where $2n$ is the number of plies in the laminate).

To quantify this energy absorption we first calculate the variation of ply fracture energy with angle, and then calculate the delamination area and associated energy.

Present address: B.P. Research, Sunbury-on-Thames, Middlesex TW16 7LN, UK.

0022–2461/87 $03.00 + .12

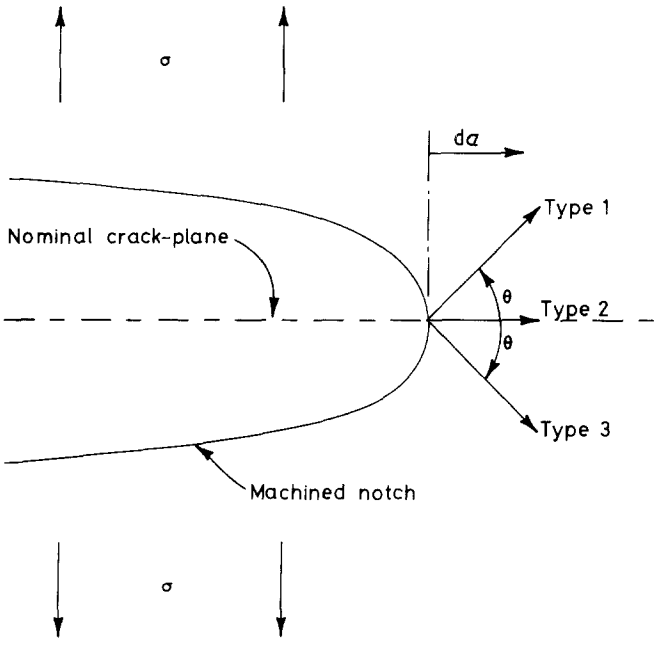

Figure 1 Schematic illustration of notch-tip crack formation in a composite laminate.

2.1. Calculation of the off-angle fracture energy of a single ply

McGarry and Mandell [6] conducted experiments on woven glass/epoxy material, and found the energy absorption for a crack running at $\theta°$ from the perpendicular to the loading direction is given by:

$$G(\theta) = G(0) \cos \theta \quad (1)$$

where $G(0)$ is the energy absorption per unit area of crack surface at $\theta = 0°$, and may be calculated by models of toughening [4, 5]. This equation implies that the energy to fracture each fibre is constant, since the cosine term reflects a reduced number of fibres broken by an angled crack.

Piggott [7] analysed the case of isolated fibres toughening a matrix, and found:

$$G(\theta) = G(0)\,(1 - 2.4A \tan \theta) \quad (2)$$

where A is a non-dimensional parameter depending on the force exerted by the matrix on the fibre ($A = 0.083$ for E-glass/epoxy).

The predictions of Equations 1 and 2 are similar, although the validity of Equation 2 is unknown in the light of the revised models of toughness discussed by Wells and Beaumont in a previous publication [5]. For simplicity, Equation 1 has been used.

The energy absorbed when a crack advances a distance δx (measured perpendicular to the loading direction) breaking fibres aligned at an angle ϕ to the loading direction is (see Fig. 3):

$$W = \frac{G(0)|\cos(\theta + \phi)|t\delta x}{\cos \theta} \quad (3)$$

where t is the ply thickness.

2.2. Calculation of the delamination energy

The energy absorbed in delamination is the product of the area of delamination and the interlaminar toughness. Dorey *et al.* [8] impact loaded composite plates, producing extensive delamination. They found the interlaminar toughness (in shear), G_d, to be about $700\,J\,m^{-2}$, from correlations in the residual shear strength and delaminated areas of the material and is the value used in this paper. This value is consistent with other values reported [9].

The energy of delamination, found by simple geometry outlined in the example shown in Fig. 4 is

$$W = 2da G_d \delta x \tan \theta \quad (4)$$

2.3. Modifications to the model at small crack openings

When a damage zone is small, the opening of the crack is also small and fibre fracture and complete pull-

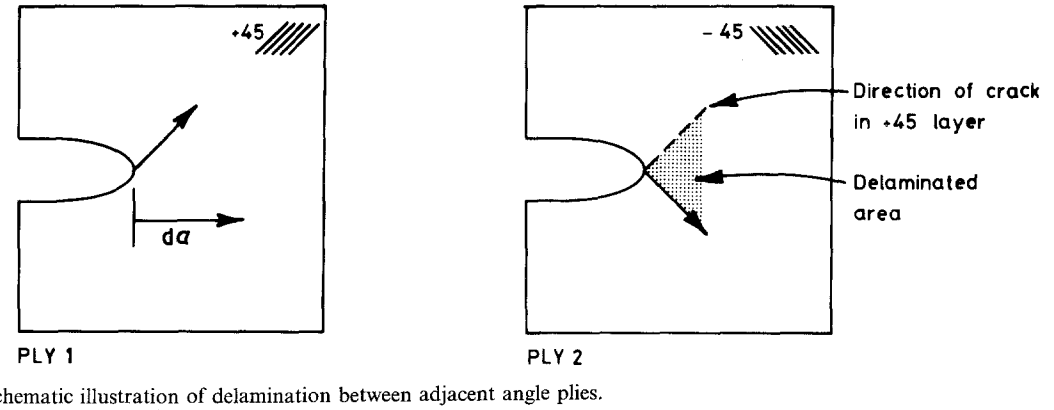

Figure 2 Schematic illustration of delamination between adjacent angle plies.

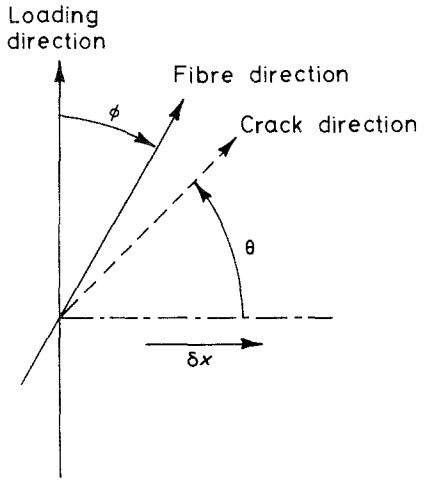

Figure 3 Co-ordinate system used in the model.

out may not occur. In this case the maximum toughening due to the mechanisms described by Wells and Beaumont [5] will not be attained. The interfacial and elastic energy will be completely absorbed only on fibre fracture, and the crack advance at which this occurs must therefore be found. Further, the maximum pull-out energy is only developed when the crack opening is equal to the pull-out length.

Using geometrical considerations, the crack advance at which fibre fracture occurs was discussed by Wells [10] who found that simple theories did not predict the critical crack advance for fibre fracture, a_c. However, Wells [10] found experimentally that $a_c \simeq 0.5$ mm for a $(0/90)_s$ carbon/epoxy laminate and proposed that the value of a_c depended on the stiffness of the laminate in the loading direction, E_A, and the debond length, l_d, according to the approximation

$$a_c \simeq 2.22 \times 10^{-21}(E_A l_d)^2 \quad (5)$$

Larger crack advances (i.e. larger damage zones) are required to complete the pull-out process and achieve maximum toughening. Wells [10] found the critical crack advance for complete fibre pull-out is given by the approximation:

$$b_c \approx 2.4 \times 10^{-17}(E_A \bar{l}_p)^2 \quad (6)$$

Using values for $(0/90)_s$ carbon/epoxy an approximate value of 5 mm is found for b_c. Values for other materials and lay-ups are calculated using Equations 5 and 6.

Knowing the two critical crack advances, a_c and b_c, it is now necessary to reduce the value of $G(0)$ used in Equation 3 at small crack advances. This allows for the reduced energy absorption achieved in such cases.

Wells [10] showed that the energy absorbed in elastic and interfacial work prior to fibre fracture is roughly proportional to $(da/a_c)^{1/2}$, and the pull-out work approximately proportional to (da/b_c). The toughness $G'(da)$ is therefore given by the approximations:

$$G'(da) = G(0)\left[(1-\alpha)\left(\frac{da}{a_c}\right)^{1/2} + \alpha\frac{da}{b_c}\right] \quad (7)$$

for $da \leqslant a_c \leqslant b_c$, where α is the proportion of the total energy absorption due to pull-out toughening contributions. The first term, therefore, relates to the toughening due to elastic and interfacial terms and the second relates to pull-out toughening contributions.

For cases where $da > a_c$, only the pull-out contribution is reduced, and is given by:

$$G'(da) = G(0)\left[(1-\alpha) + \alpha\frac{da}{b_c}\right] \quad (8)$$

for $a_c < da < b_c$.

3. Calculation of R-curves

The previous section has described how the crack propagation in each laminate ply can be modelled as one of three types (or directions). These three crack types absorb different amounts of energy, since they can involve resin cracking parallel to the fibres or fracture of the fibres at various angles. In addition, fibre fracture at small crack advances absorbs less energy than at large crack advances, and if the directions of cracks in adjacent plies are not the same then delamination will occur between the plies, absorbing energy.

The model, therefore, allows the energy absorption to be calculated for all the possible cracking directions it considers, and these may readily be calculated by computer. It we assume that the crack path will, in fact, follow the lowest energy path, then the model allows us to find the energy absorbed as the crack advances. This information is the same as that contained in an "R-curve" and, consequently, the results of this model are presented in this form.

An R-curve shows the variation of absorbed energy

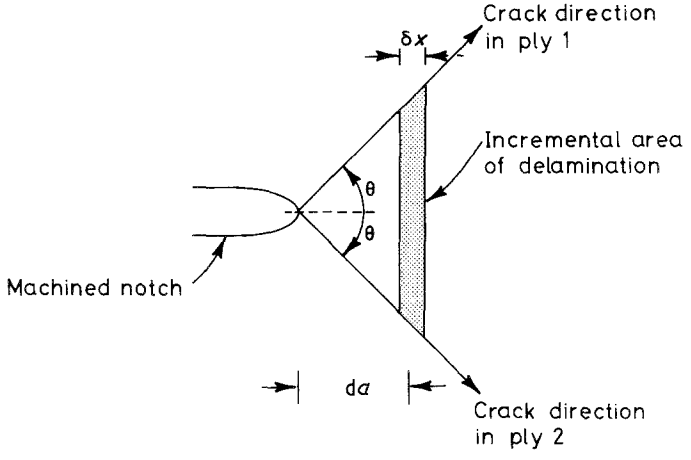

Figure 4 Incremental area of delamination between adjacent angle-plies.

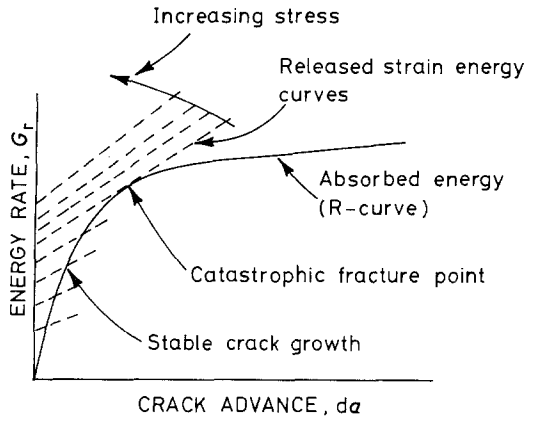

Figure 5 Determination of fracture stress from an R-curve.

with damage zone size. The strength of the notched material, and the size of the damage zone at fracture, may be found by plotting released strain energy curves as shown in Fig. 5, which are given by: $K_r = \sigma[\pi(a + da]^{1/2} = (EG_r)^{1/2}$.

At low applied stresses the released elastic energy is greater than that absorbed and the damage zone grows (stably) until the two are equal. At some critical stress/crack length combination the strain energy release rate is always greater than that absorbed, and catastrophic failure occurs. This is defined by the point of tangency between the released and absorbed energy curves.

3.1. Material properties used in the model

The R-curve model described may be used for laminates of various materials, using lamina properties listed in Table I. The values of G, $\bar{l}_p$, l_d and α for individual laminae are taken from Wells [10], and the elastic values are typical reported values for the materials.

The values of a_c and b_c are calculated from the equations given in Section 2.3. The estimates of a_c and b_c are very approximate, and strictly apply to single fibre debonding and pull-out only. However, in CFRP, a_c is estimated using the bundle debond length and b_c with the bundle pull-out length, since single fibre processes are essentially absent in this material [5].

3.2. Conversion of G prediction to K notation

Experimental data for comparison with the predicted R-curves is available only in stress intensity factor form. The model in this work predicts the behaviour in terms of energy absorption and hence gives data in G form. For isotropic materials the two parameters are related by the material Young's modulus, E, by

$$K = (EG)^{1/2}$$

However, for anisotropic materials, an effective stiffness, E', must be used and has been calculated by Sih *et al.* [11]. They showed that for mode 1 failure of a crack perpendicular to the load direction which is applied along the 1 direction

$$E' = \left|\left(\frac{a_{11}a_{22}}{2}\right)^{1/2}\left[\left(\frac{a_{22}}{a_{11}}\right)^{1/2} + \frac{2a_{12} + a_{66}}{2a_{11}}\right]^{1/2}\right|^{-1}$$

where the a_{ij} are elements of the laminate compliance matrix. This relationship only strictly applies to self-similar cracking.

The axial modulus, E_A, and the effective modulus E', Table II, are calculated from the lamina elastic properties shown in Table I.

4. Comparison of predictions with experimental data

The first reported R-curve determination for composites was made by Gaggar and Broutman [12] on chopped glass fibre in epoxy and polyester matrices. There is also a limited amount of data for high strength carbon/epoxy laminates. Morris and Hahn [13] and Ochiai and Peters [14] conducted tensile tests on notched specimens, whilst Kim [15] used both tensile and three-point bending geometries. All the investigators used a crack opening displacement (COD) clip gauge to determine the crack advance, da.

As noted in Section 3.2 the effective modulus derived by Sih *et al.* [11] applies only to self-similar cracking, which the processes occurring at the notch tip are manifestly not. The energy is absorbed by a combination of fibre fracture, at a variety of orientations, and delamination energy. Although the Sih effective modulus, E', is a useful first attempt, the true relationship between K_I and G_I for the mode of cracking involved is non-trivial. In this work an empirical linear combination (E'') of laminate axial modulus and Sih effective modulus is used, given by:

$$E'' = \tfrac{2}{3}E_A + \tfrac{1}{3}E'. \quad (9)$$

Figs 6 to 9 show the collected published R-curve data for composite laminates together with the model predictions using both effective moduli E' and E''. For quasi-isotropic laminates $E' = E''$. The second choice of modulus, E'', appears to give better agreement for the range of laminates which have differing anisotropy.

The model correctly predicts the sharply increasing energy absorption as the crack advances, reaching an almost constant value at larger crack advances when fibre fracture occurs. This suggests that the estimate of the critical crack advance for fibre fracture, a_c, was

TABLE I Values of lamina properties in R-curve prediction

Fibre type	G (kJ m^{-2})	α (%)	$\bar{l}_p$ (mm)	l_d (mm)	E_1 (GPa)	E_2 (GPa)	G_{12} (GPa)	ν_{12}
E-glass	61	23	0.21	3.8	35	5	1.9	0.3
Kevlar	240	73	0.71	7.2	76	5.5	2.1	0.34
High-modulus carbon	19	3	0.09	2.9	220	9.8	5.3	0.34
High-strength carbon	67	6	0.22	7.7	140	9.8	5.3	0.34

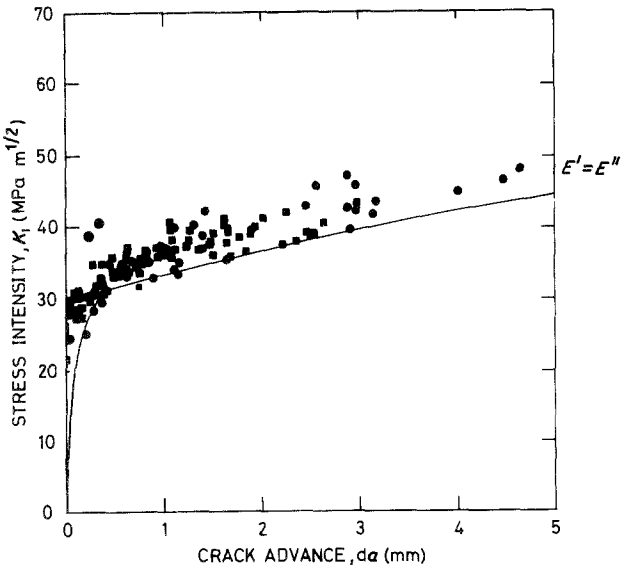

Figure 6 R-curve data for quasi-isotropic CFRP laminates. (●) Morris and Hahn [13] $(0/45/-45/90)_s$; (■) Kim [15] $(0/90/45/-45)_s$.

fairly accurate. Fig. 6 shows a rising energy absorption curve even at large crack advances. This is due to the increasing amount of delamination area required by the fracture path. The model predicts that the lowest energy path is crack orientations of $+45°$, $+45°$, $-45°$, $90°$ in the $(0/\pm45/90)_s$ laminate, which has delamination between plies to accommodate the three different cracking directions.

The agreement between predicted and observed R-curves is good. The results of Ochiai and Peters do not extend to large damage zone sizes because of the restricted range of notch sizes employed, and the small slope of the curve in (0/90) laminate.

4.1. Predicted R-curves for other materials.

Energy absorption curves have been calculated for four common lay-ups of the four composite systems listed in Tables I and II. The results, in the form of G against da curves, are shown in Fig. 10. The abbreviations G, K, HM and HS refer to E-glass, Kevlar, high-modulus and high-strength carbon fibre-reinforced epoxy laminates, respectively. Kevlar shows a consistently high energy absorption, but its long pull-out length (and reliance on pull-out for toughening) mean that it rarely attains its maximum toughness at the onset of catastrophic failure which roughly corresponds to the point $da = a_c$.

The R-curves are replotted in Fig. 11 in K_I against da form, using the modulus E'' defined in Equation 9 and given in Table III. The effect of introducing the stiffness is to change the relative positions of the different materials, notably high-modulus carbon, the high stiffness of which compensates for its low toughness.

TABLE III Laminate properties. The upper figure is the effective modulus E'' (GPa), the lower is the ultimate laminate strength (MPa)

	Glass	Kevlar	Carbon	
			High-mod.	High-strength
$(0/90)_s$	17.3 350[1]	33.2 590[2]	92.7 490[2]	62.8 780[5]
$(0/\pm45)_s$	14.7 367[2]	27.4 413[2]	76.9 353[2]	53.0 617[6]
$(0/\pm45/0)_s$	17.5 475[2]	34.2 635[2]	96.9 495[2]	65.0 932[7]
$(0/\pm45/90)_s$	14.9 303[3]	28.8 394[4]	80.9 289[2]	54.3 494[8]
$(\pm45)_s$	8.1 146[4]	11.0 119[4]	28.8 170[2]	25.0 170[2]

Notes:
1. Average of values from McGarry and Mandell [6] and Nuismer and Whitney [17].
2. Calculated by laminated plate analysis, using values in Table I.
3. Average values from Zweben [18] ("tape" value) and Nuismer and Whitney [17].
4. From Zweben [18] ("tape" value).
5. Average of values from Ochiai and Peters [14] and Nuismer and Whitney [17].
6. Average of values from Potter [19], Bishop [20] and Morris and Hahn [13].
7. From Ochiai and Peters [14].
8. Average of values from Whitney and Kim [21] and Nuismer and Whitney [17].

4.2. Deduced notch strength of laminates

The notched strength of a laminate, σ, may be deduced from Figs 10 and 11 using the tangency method described in Section 3. This is done by plotting "released" K curves for a variety of stress levels for a single crack length, a. The tangency condition then yields the notched strength, σ, as a function of crack length, a. The R-curve predictions are compared with notch strength data collected for a wide variety of lay-ups and fibre reinforcements [16] (Fig. 12).

4.2.1. Carbon $(0 \pm 45)_s$ material

Fig. 13 shows data from Fig. 12 for carbon-fibre composites of $(0/\pm45)_s$ and $(\pm45/0)_s$ lay-ups. The R-curve model predicts identical notched strengths for the two materials. Predictions for high-modulus and high-strength carbon fibres are shown. The material

TABLE II Stiffness values (GPa) for common lay-ups of various materials

Fibre type	$(0/90)_s$		$(0/\pm45)_s$		$(0/\pm45/90)_s$		$(0/\pm45/0)_s$		$(\pm45)_s$	
	E_A	E'	E_A	E'	E_A	E'	E_A	E'	E_A	E'
E-glass	20.2	11.4	16.2	11.6	14.9	14.9	21.0	10.6	6.5	11.4
Kevlar	41.0	17.7	30.8	20.7	28.8	28.8	42.3	18.4	7.6	17.7
High-modulus carbon	115.4	47.4	87.1	56.4	80.9	80.9	120.8	49.1	19.5	47.4
High-strength carbon	75.4	37.5	59.7	39.6	54.3	54.3	80.1	34.9	18.7	37.5

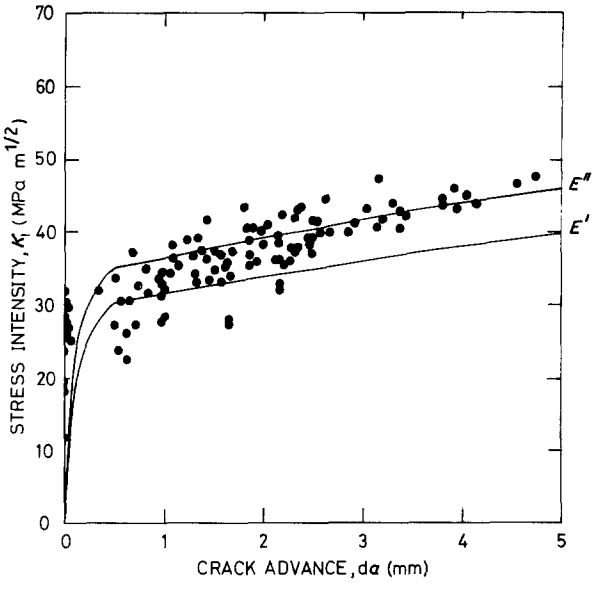

Figure 7 R-curve data for $(0/\pm 45)_s$ CFRP laminates.

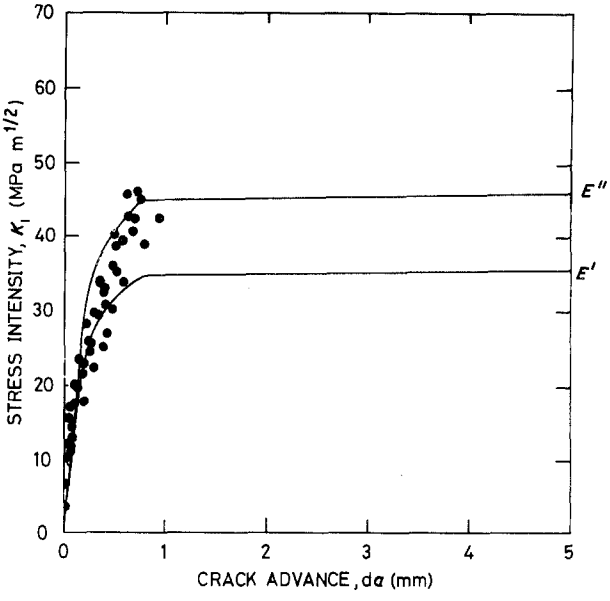

Figure 8 R-curve data for $(0/90)_s$ CFRP laminates.

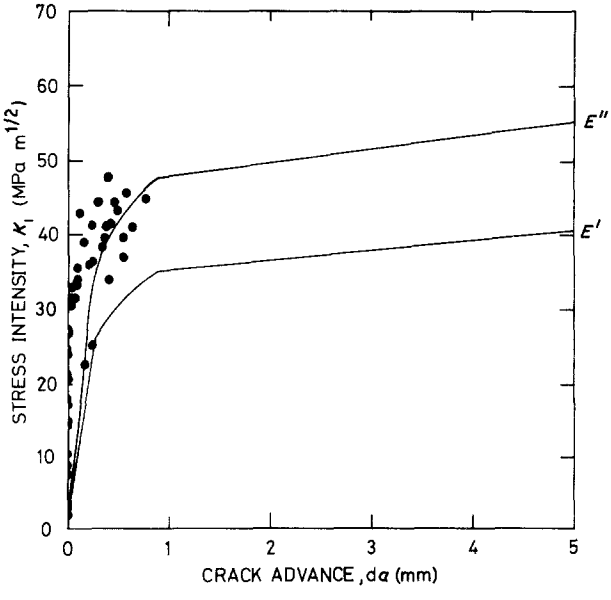

Figure 9 R-curve data for $(0/\pm 45/0)_s$ CFRP laminates.

tested was generally of high- or intermediate-strength type, and is unlikely to have properties exactly as used in the model. The predictions for both types of fibres, therefore, give some estimate of the scatter band in which the data might be expected to fall.

The predictions agree well with the data. The average of the normalized fracture toughnesses predicted at crack lengths of 2, 5, 10 and 15 mm are:

$$\text{high strength} \quad \frac{K_{Ic}^*}{\sigma_u} = 0.058 \pm 0.006\,m^{1/2}$$

$$\text{high modulus} \quad \frac{K_{Ic}^*}{\sigma_u} = 0.074 \pm 0.013\,m^{1/2}$$

The average value of K_{Ic}^*/σ_u is an indication of the notch-sensitivity of the material. The standard deviations give an indication of how much the fracture toughness changes with crack length. If the errors are small, then standard linear elastic fracture mechanics (LEFM) may be used to predict the notched strength.

4.2.2. Other lay-ups of carbon-fibre material

Fig. 14 shows data for $(0/\pm 45/90)_s$ and Fig. 15 for $(0/+45/0/-45)_s$ material, taken from Fig. 12. Agreement between the data and the two predictions is again satisfactory. The average normalized fracture toughness (found as before) is:

	$(0/\pm 45/90)_s$	$(0/\pm 45/0)_s$
high strength		
$\frac{K_{Ic}^*}{\sigma_u}$	$0.065 \pm 0.009\,m^{1/2}$	$0.048 \pm 0.003\,m^{1/2}$
high modulus		
$\frac{K_{Ic}^*}{\sigma_u}$	$0.094 \pm 0.010\,m^{1/2}$	$0.070 \pm 0.006\,m^{1/2}$

The difference in notch-sensitivity between these three constructions of carbon-fibre material are successfully predicted by the model.

4.2.3. Kevlar $(0/\pm 45/90)_s$

Fig. 16 shows the data (from Fig. 12) and predictions for Kevlar $(0/\pm 45/90)_s$ material. Agreement with the limited data is good; the average of the predicted normalized fracture toughness is

$$\frac{K_{Ic}^*}{\sigma_u} = 0.072 \pm 0.015\,m^{1/2}$$

This is similar to the normalized fracture toughness for high-strength carbon fibre of the same construction, despite the much higher total toughness of Kevlar.

4.2.4. Glass $(0/90)_s$ and $(0/\pm 45/90)_s$

Data and corresponding predictions for two lay-ups of glass material are plotted in Fig. 17. Agreement is good with the prediction where:

$$K_{Ic}^*/\sigma_u = 0.058 \pm 0.008\,m^{1/2} \quad (0/\pm 45/90)_s$$

$$K_{Ic}^*/\sigma_u = 0.063 \pm 0.002\,m^{1/2} \quad (0/90)_s$$

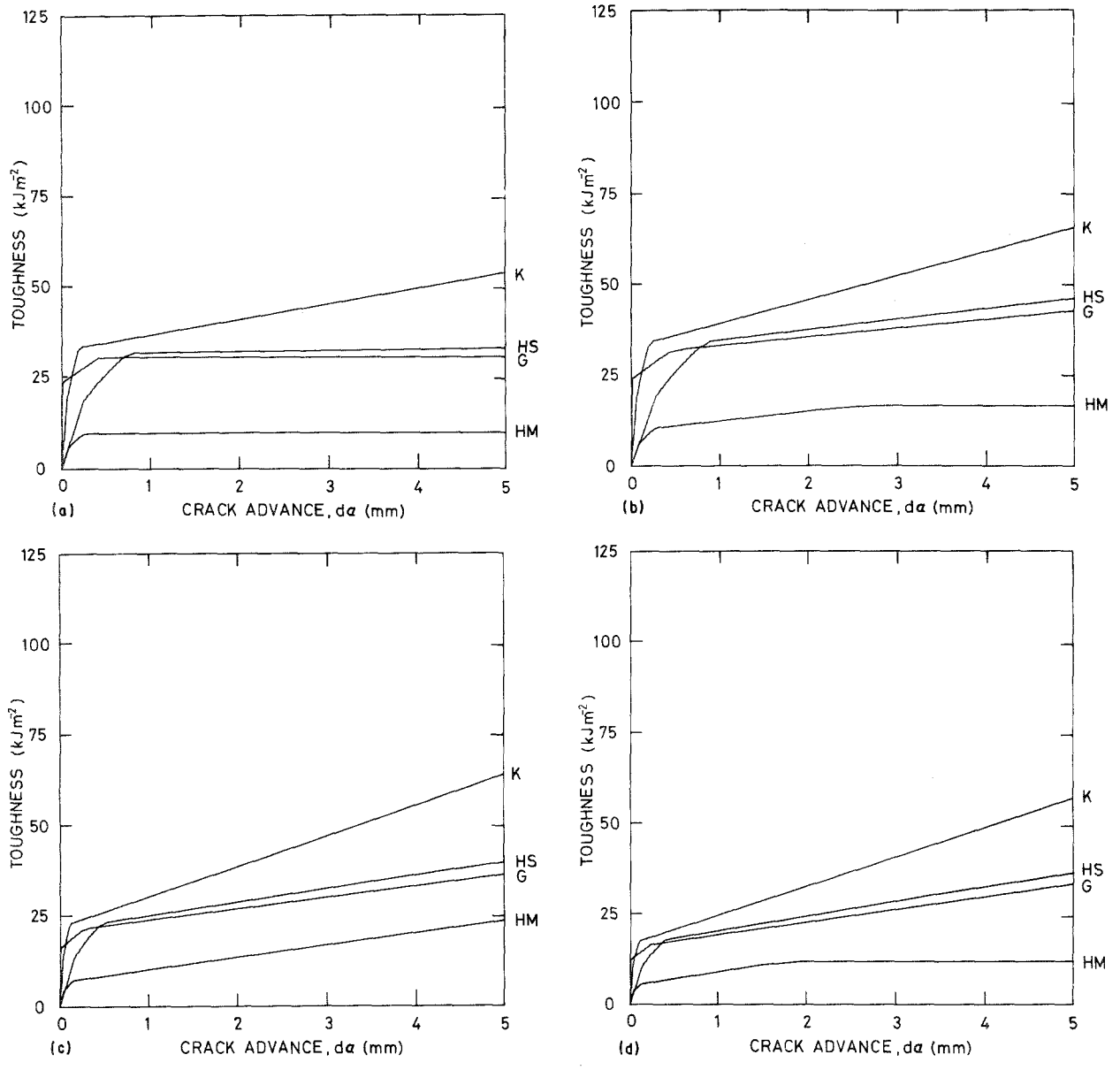

Figure 10 Calculated R-curves in toughness/crack advance form for four common lay-ups of four fibre types: E-glass (G), Kevlar (K), high-modulus carbon (HM) and high-strength carbon (HS). (a) $(0/90)_s$, (b) $(0/45/-45/0)_s$, (c) $(0/45/-45)_s$, (d) $(0/45/-45/90)_s$.

5. R-curves for "notch-insensitive" lay-ups

Certain lay-ups of composite laminates are said to be "notch-insensitive", the most common example is $(\pm 45)_s$. Notch insensitivity implies the notch has no other effect than to reduce the cross-sectional area of the specimen. The failure stress of a specimen, of width w, with a central notch of length $2a$, is then given by:

$$\sigma = \left(1 - \frac{2a}{w}\right)\sigma_u \qquad (10)$$

Failure is due to the fracture of the remaining material at its ultimate strength ("net-section failure").

An R-curve for a $(\pm 45)_{2s}$ laminate has been calculated to investigate the reason for this notch insensitivity (Fig. 18). The large scale for damage zone size should be noted. An angle-ply laminate, such as $(\pm 45)_{2s}$, attempts to fracture in a "1313" mode. This is achieved by pure splitting in which the energy absorption is low, but has to be off-set against the need to delaminate a triangular area between the two splits. The energy absorption is dominated by this delamination energy, which rises linearly with the crack advance.

At some point the energy absorbed by delamination is equal to the energy which would be absorbed in propagating a crack (in a Type 2 direction) through both plies. At this point, the cracks change direction and the energy absorption attains a constant value. The change in crack direction is predicted to occur at da values of $da \simeq 8$ mm for glass, > 25 mm for Kevlar, ~ 3 mm for high-modulus carbon, and ~ 8 mm for high-strength carbon.

Following the method described in Section 4.2, and using the values in Table III, the notched strength of $(\pm 45)_{2s}$ laminates in all four materials, was found (Fig. 19). The figure also shows lines of net-section failure for different specimen widths, calculated from Equation 10. Since the net-section stress forms an upper bound on the notched strength, $(\pm 45)_{2s}$ laminates will be notch-insensitive in narrow specimens. However, the material is not unconditionally notch-insensitive; for suitable plate widths and notch

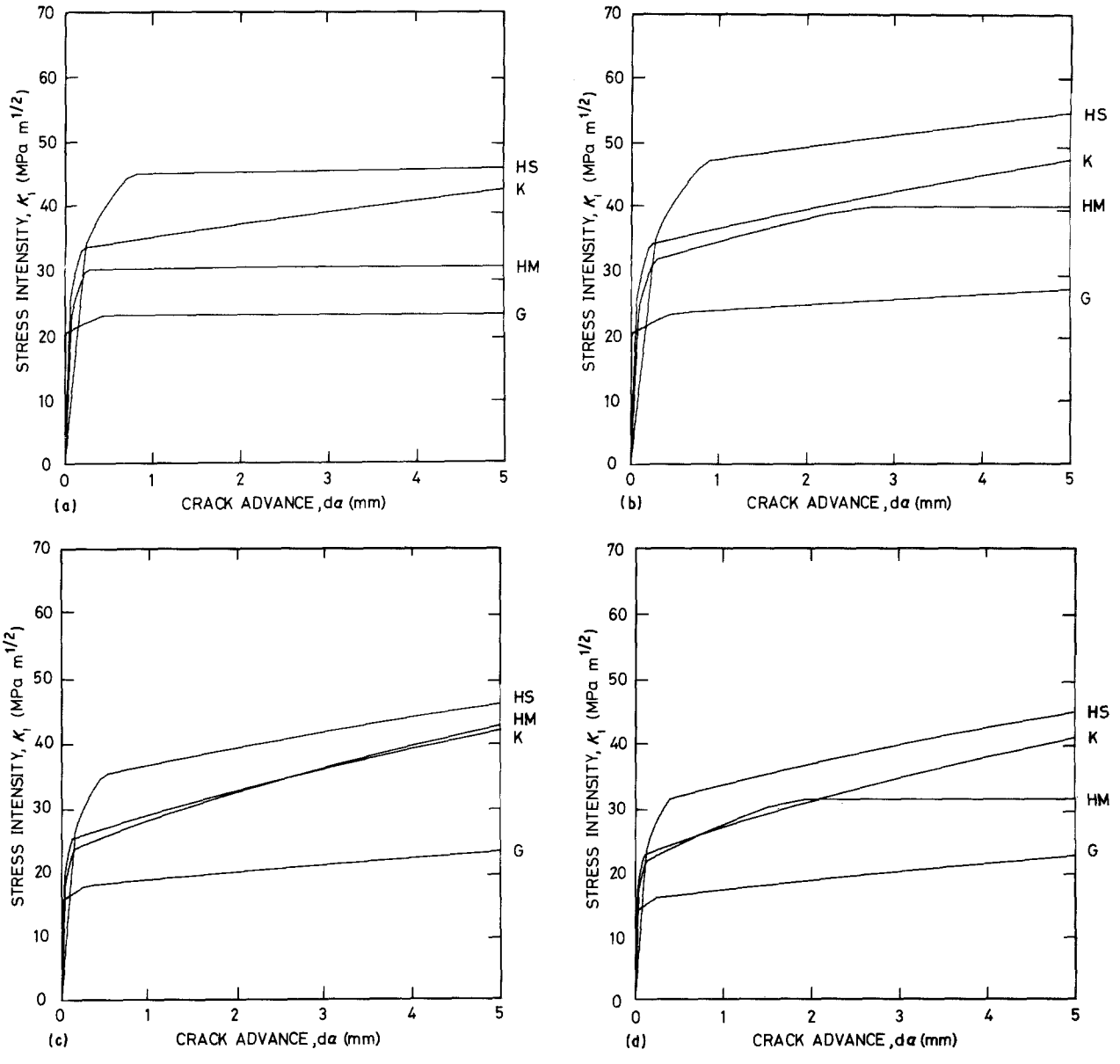

Figure 11 Calculated R-curves in stress intensity/crack advance form for four common lay-ups of four fibre types (key as Fig. 10). (a) $(0/90)_s$, (b) $(0/45/-45/0)_s$, (c) $(0/45/-45)_s$, (d) $(0/45/-45/90)_s$.

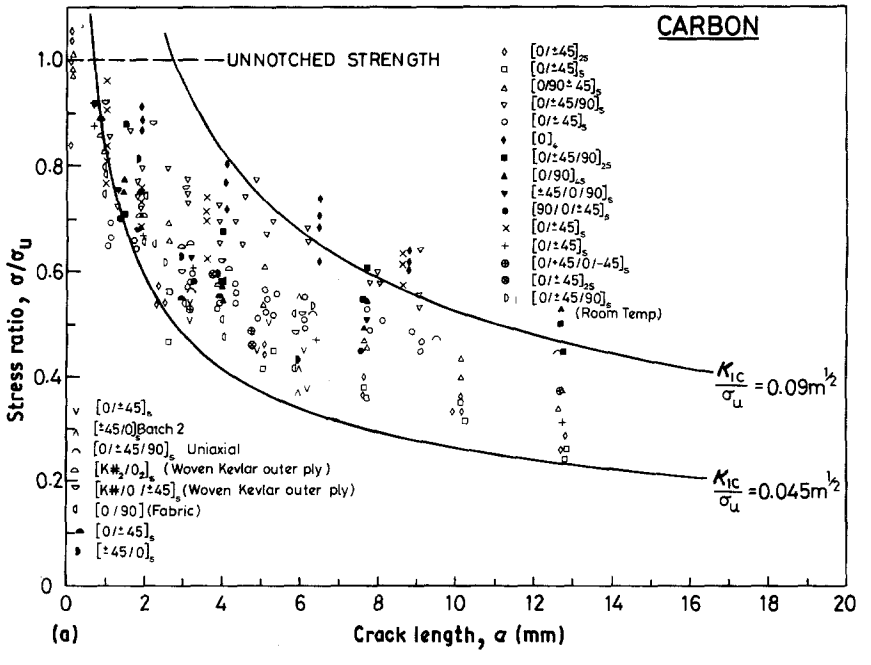

Figure 12 Variation of stress ratio, σ/σ_u, with crack length for (a) carbon, (b) glass and (c) Kevlar composites. The curves are compiled from the data given by Wells and Beaumont [16].

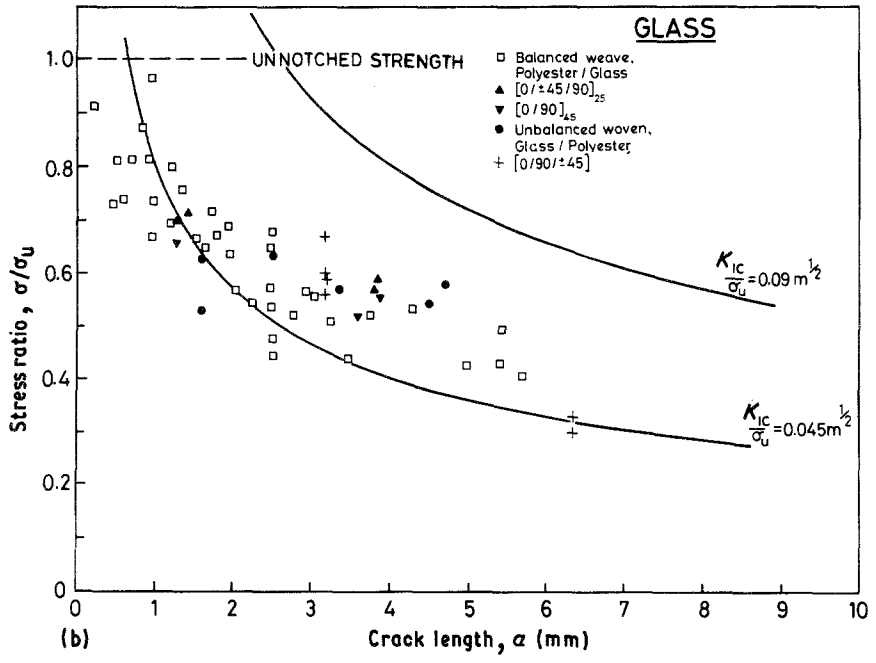

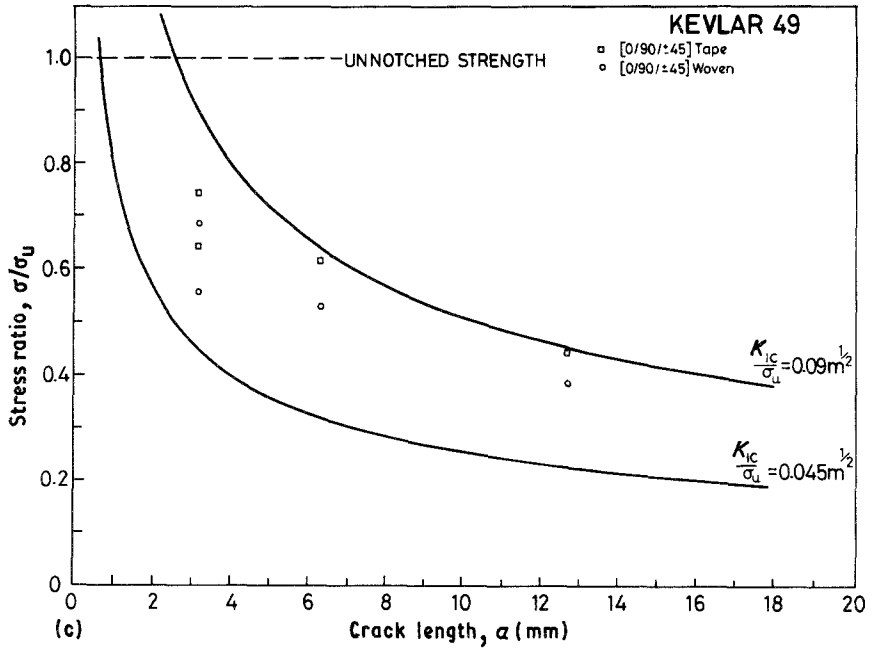

Figure 12 Continued

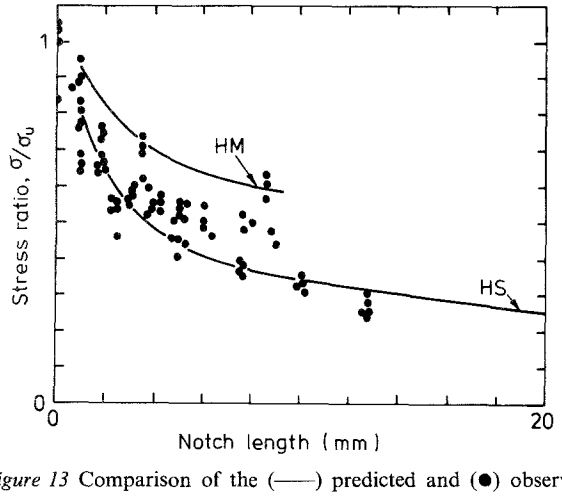

Figure 13 Comparison of the (——) predicted and (●) observed notched strength of CFRP $(0/\pm 45)_s$ and $(\pm 45/0)_s$ materials.

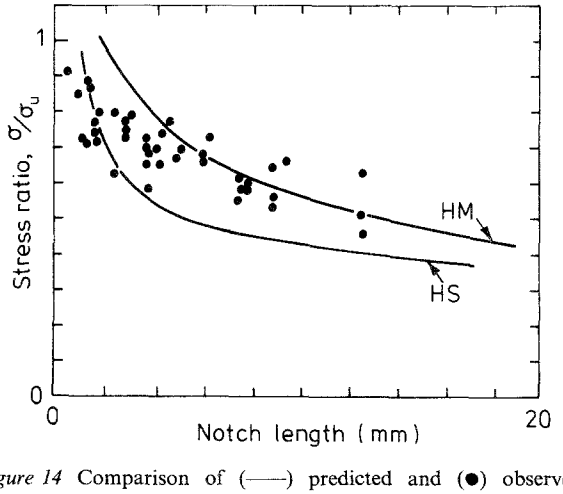

Figure 14 Comparison of (——) predicted and (●) observed notched strengths of CFRP $(0/\pm 45/90)_s$ material.

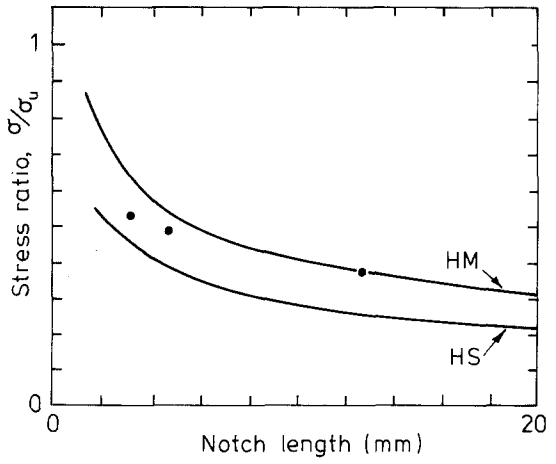

Figure 15 Comparison of (——) predicted and (●) observed notched strengths of CFRP $(0/+45/0/-45)_s$ material.

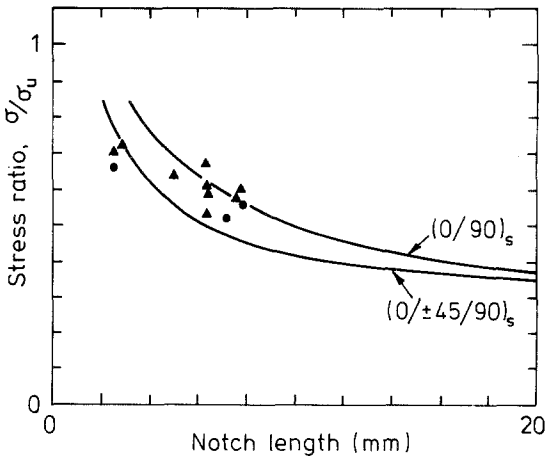

Figure 17 Comparison of (——) predicted and observed notched strengths of GFRP $(0/90)_s$ (▲) and $(0/\pm45/90)_s$ (●) materials.

lengths, the failure stress may be significantly lower than the net-section failure stress.

Sections of angle-ply lay-ups are incorporated into "notch sensitive" laminates to act as "crack barriers". This model enables some estimates to be made of the maximum effective width of such a "barrier strip". Under certain circumstances, the material may not be notch-insensitive as expected.

The parameter K_{Ic}^*/σ_u, discussed in Section 4.2, no longer attains a constant value at short crack lengths. Instead, it continues to rise to a much higher value at very long crack lengths.

6 Case studies

6.1. Effect of fibre surface treatment

Lee and Phillips [22] investigated the notched strength of composites in detail, testing a large number of lay-ups and material types. They found a high strength carbon $(0/90)_{2s}$ laminate to have unusually high notch-sensitivity when the fibres had received surface treatment to produce a good interfacial bond. This was in contrast to the low notch-sensitivity of a $(0/\pm45/0)_s$ lay-up of high-modulus carbon material.

The notched strength of the high strength carbon $(0/90)_s$ material has been predicted using the methods described by Wells and Beaumont [4, 5], and is shown in Fig. 20. The bond between fibre and matrix was known to be enhanced for these fibres, and a value of $G_I = 250\,J\,m^{-2}$, four times the normal value, was used for the interfacial toughness. This implies an increase in interfacial shear strength by a factor of $\sqrt{4} = 2$. The toughness of the unidirectional lamina was found to be described by: $G = 20\,kJ\,m^{-2}$, $\alpha = 1.4\%$, $\bar{l}_{pb} = 0.06\,mm$, and $l_{db} = 2.1\,mm$. The R-curve has been calculated using the moduli for high-strength carbon $(0/90)_s$ quoted in Tables II and III.

Fig. 20 shows good agreement between prediction and data. The figure also shows the predicted strength for the (0/90) material with a normal bond strength ($G_I = 61\,J\,m^{-2}$). The material is significantly less notch-sensitive than the well-bonded case. The predicted fracture toughness of $42.4 \pm 2.5\,MPa\,m^{1/2}$ is in excellent agreement with the value of $43.0\,MPa\,m^{1/2}$ reported by Lee and Phillips for the "normal" material. The predicted strength of the high modulus carbon $(0/\pm45/0)$ material (deduced from Fig. 11) also agrees closely with the data; net-section failure occurring at long notch lengths.

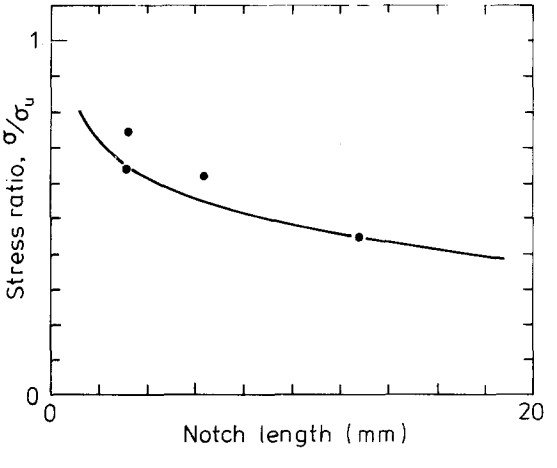

Figure 16 Comparison of (——) predicted and (●) observed notch strengths of quasi-isotropic Kevlar-reinforced plastic laminates $(0/90/\pm45)_s$.

7. Conclusions and implications

A simple model has been derived to predict R-curves

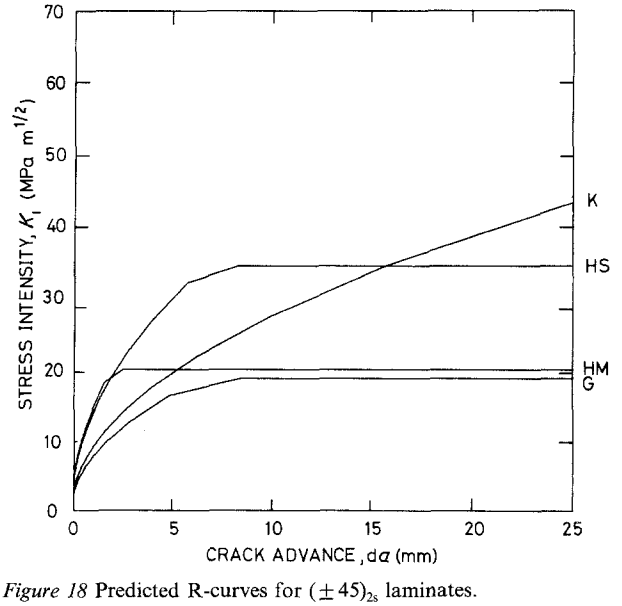

Figure 18 Predicted R-curves for $(\pm45)_{2s}$ laminates.

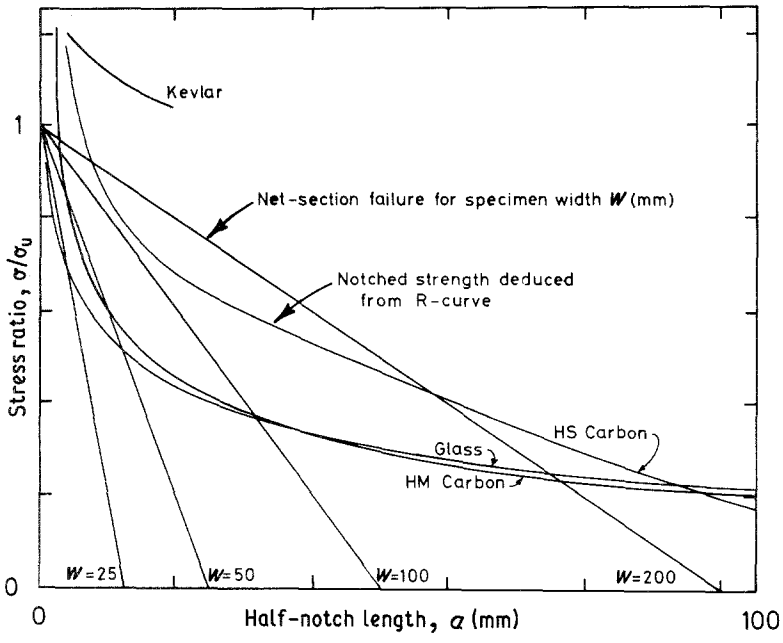

Figure 19 Predicted notched strengths of $(\pm 45)_{2s}$ laminates of glass, Kevlar, high-modulus and high-strength carbon fibre. The lines of net-section failure for a specimen of width W (mm) are also shown.

for laminates and is found to be in reasonable agreement with published R-curve data. The model enables the fracture toughness and notched tensile strength of a laminate to be calculated from the properties of the fibre, matrix and interface. For "notch-sensitive" laminates, a normalized apparent fracture toughness, K_{Ic}^*/σ_u, of about $0.065\,m^{1/2}$ is predicted for all fibre types which is in good agreement with experimental values. The model can also explain the "notch-insensitivity" of angle-ply laminates and "notch-sensitivity" of strongly-bonded laminates.

The model, despite its simplicity, accounts for the detailed differences in notch-sensitivity between different laminate constructions. Taking the parameter K_{Ic}^*/σ_u as a measure of notch-sensitivity, the results for typical materials may be summarized.

1. Laminates containing a high proportion of 0° fibres (e.g. $(0/90)_s$, $(0/\pm 45)_s$ and $(0/\pm 45/0)_s$ are notch-sensitive with little variation of fracture toughness with initial notch length). The notched strength may be accurately predicted using the methods of LEFM.

2. Laminates with a lower proportion of 0° fibres, and containing angle-plies (e.g. $(0/\pm 45/90)_s$) exhibit intermediate notch-sensitivity. The normalized fracture toughness is higher than in class 1, and varies with the crack length. The methods of LEFM may only be used with caution.

3. Laminates in classes 1 and 2 show relatively small changes in notch-sensitivity when the type of fibre reinforcement is changed.

4. Pure angle-ply laminates (e.g. $(\pm 45)_s$) are commonly notch-insensitive (see Section 5), when the methods of LEFM are invalid.

5. The notch-insensitivity will also be affected by factors such as interlaminar shear strength and laminar toughness.

Acknowledgements

The authors wish to acknowledge useful discussions with Professor M. F. Ashby. One of us (J. K. W.) acknowledges the support of the S.E.R.C. during the course of the work.

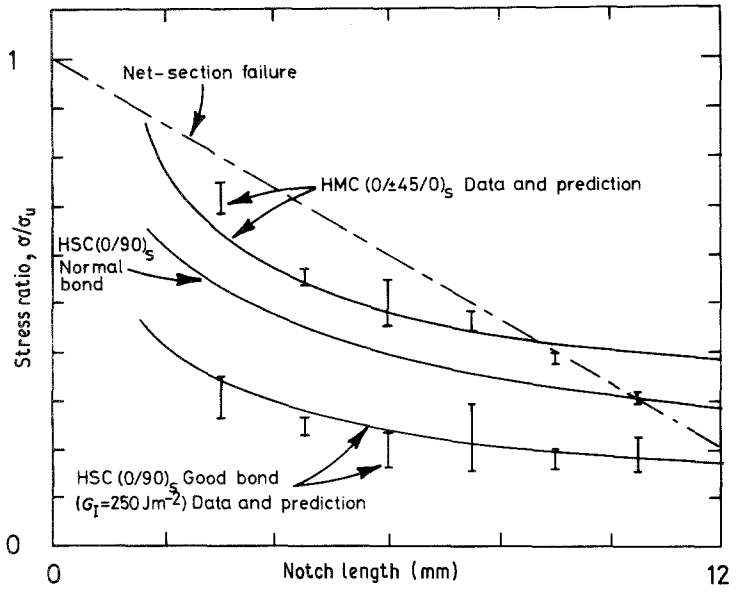

Figure 20 Comparison of predicted notched strengths with the data of Lee and Phillips [22].

References

1. J. M. WHITNEY and R. J. NUISMER, *J. Comp. Mater.* **8** (1974) 253.
2. R. B. PIPES, R. C. WETHERHOLD and J. W. GILLESPIE, *Mat. Sci. Engng* **45** (1980) 247.
3. M. E. WADDOUP, J. R. EISENMANN and B. E. KAMINSKI, *J. Comp. Mater.* **5** (1971) 446.
4. J. K. WELLS and P. W. R. BEAUMONT, *J. Mater. Sci.* **20** (1985) 1275.
5. *Idem, ibid.* **20** (1985) 2735.
6. F. J. McGARRY and J. F. MANDELL, "Special discussion on Solid–Solid Interfaces" (Chemical Society, Nottingham, 1972).
7. M. R. PIGGOTT, *J. Mech. Phys. Solids* **22** (1974) 457.
8. G. DOREY, G. R. SIDEY and J. HUTCHINGS, *Composites* **9** (1978) 25.
9. G. R. SIDEY and F. J. BRADSHAW, Paper 25, Proceedings of the First International Carbon Fibre Conference, London. (Institute of Physics, 1971).
10. J. K. WELLS, PhD Thesis, Cambridge University (1982).
11. G. C. SIH, P. C. PARIS and G. R. IRWIN, *Int. J. Fract. Mech.* **1** (1965) 189.
12. S. GAGGAR and L. J. BROUTMAN, *J. Comp. Mater.* **9** (1975) 216.
13. D. H. MORRIS and H. T. HAHN, ASTM STP 617 (American Society for Testing and Materials, Philadelphia, Pennsylvania, 1977) p. 5.
14. S. OCHIAI and P. W. M. PETERS, *J. Mater. Sci.* **17** (1982) 417.
15. R. Y. KIM, *Exp. Mech.* **19** (1979) 50.
16. J. K. WELLS and P. W. R. BEAUMONT, *Scripta Metall.* **16** (1982) 99.
17. R. J. NUISMER and J. M. WHITNEY, ASTM STP 593 (American Society for Testing and Materials, Philadelphia, Pennsylvania, 1975) p. 117.
18. C. ZWEBEN, ASTM Symposium on "Composite Fracture Mechanics", Gaithersburg, USA (American Society for Testing and Materials, Philadelphia, Pennsylvania, 1974).
19. R. T. POTTER, *Proc. Roy. Soc. Lond.* **A361** (1978) 325.
20. S. M. BISHOP, RAE TR 77093 (HM Stationary Office, London, 1970).
21. J. M. WHITNEY and R. Y. KIM, ASTM STP 617 (American Society for Testing and Materials, Philadelphia, Pennsylvania, 1977), p. 229.
22. R. J. LEE and D. C. PHILLIPS, Proceedings of the First International Conference on Composite Structures, edited by I. M. Marshall (Butterworth Scientific Press, Paisley, Scotland, 1981).

Received 2 June
and accepted 18 August 1986